Investigating non-standard sources of parity violation at the LHC

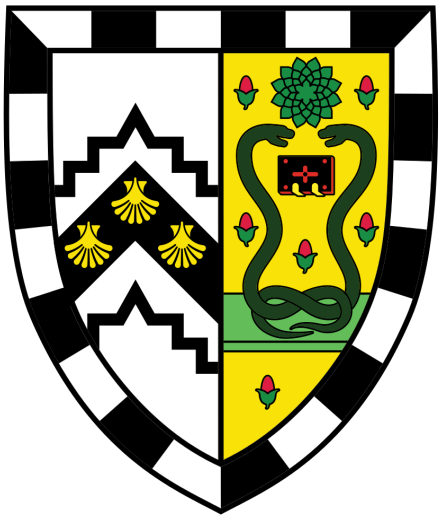

Radha Mastandrea

Gonville and Caius College

Supervisor: Prof. Christopher Lester

This thesis is submitted for the degree of

Master of Philosophy

University of Cambridge

August 16th, 2021

Rev. October 26th, 2021

Declaration

This thesis is the result of my own work and includes nothing which is the outcome of work done in collaboration except where specifically indicated in the text.

Abstract

We explore data-driven methods of detecting parity violation at particle colliders, specifically for LHC-like events where the initial states do not have a defined parity. We focus on the practical use of a predefined set of *parity variables*, which are pseudoscalars calculated on a collision event's mother and daughter particle 4-momenta. These variables claim to determine whether the physics in a given process is *chiral*, even if the underlying theory is not known. We first evaluate the usefulness of the set of parity variables on a toy model of physics designed to violate parity through a single parameter and find that the variables are indeed able to flag chirality. We also attempt to use the parity variables to explore the feasibility of detecting BSM physics in proton-proton collisions at the LHC. We introduce the Lorentz-violating minimal Standard Model Extension (mSME) and show that it has the capabilities to violate parity in the quark sector. We then test the parity variables on two mSME-motivated collider simulations, but do not find a convincing link between the mSME couplings and an observable signal in the parity variables.

Acknowledgments

The writer would particularly like to thank Dr. Christopher Lester for his mentorship over the course of the year. The writer also thanks Olivier Mattelaer for his help with deciphering the depths of the MadGraph codebase, as well as the Cambridge ATLAS group for their general advice.

Contents

Chapter 1

Symmetries, the Standard Model, and beyond

> *"Come on, let's celebrate. We've discovered a great principle of nature: The laws of physics are invariant across space and time. All the physical laws of human history, from Archimedes' principle to string theory, and all the scientific discoveries and intellectual fruits of our species are the by-products of this great law. Compared to us two theoreticians, Einstein and Hawking are mere applied engineers."*
>
> – Ding Yi, from *The Three Body Problem* (by Liu Cixin)

The elegance of science derives from symmetries. It is possible to write down the unique equations of motion for a ball being thrown into the air, no matter what continent the ball is being thrown on, whether it's being aimed at Cambridge or Glasgow, or whether it's thrown on a Tuesday or a Friday – the laws of physics don't depend on these things.[1]

Our best guesses at the laws of physics are encoded in the Standard Model Lagrangian. From this Lagrangian, we can write down the equations of motion for any particle or process in the quantum realm. The Standard Model encompasses all non-gravitational interactions between the 17 fundamental particles that define the tangible universe. We are extraordinarily lucky to have *one* such Lagrangian that is valid at all points in space and time. It is worth emphasizing, for just a moment, that this didn't have to be the case. Imagine a universe where the physical laws of motion were dependent on where and when a given experiment was done!

To this day, all experiments have shown that the laws of the universe are invariant with respect to displacements in direction and velocity. These continuous symmetries are known as *Lorentz symmetries*; their articulation in 1905 revolutionized all domains of physics, and

[1] This analogy works better if the reader is kind enough to ignore the Coriolis force, air resistance, etc...

Lorentz invariance was paramount to the construction the Standard Model.

However, important symmetries in physics do not have to be continuous. In the 1950's, the idea of CPT invariance came to prominence as a possible trait of the Standard Model. CPT invariance refers to a more fundamental set of three *discrete* symmetries that may be conserved. The *charge conjugation* operator ($\hat{C}$) flips the sign of all quantum numbers, effectively replacing particles with antiparticles; the *parity* operator ($\hat{P}$) operator inverts the signs of all spatial directions, exchanging between right- and left-handedness; and the *time reversal* operator ($\hat{T}$) sends the flow of time in the reverse direction.

Given a physical process that is allowed in the framework of the Standard Model, CPT invariance states that the physical process given by operating on the original one with $\hat{C}$ and $\hat{P}$ and $\hat{T}$ will produce another physical process that is allowed in the Standard Model. As an example, we can consider the allowed process of a pion π^+ decaying to an antimuon μ^+ and a neutrino ν. To be allowed in the Standard Model, the spin of π^+ must be zero, the spin of μ^+ must be right-handed, and the spin of ν must be left-handed. We will write this decay as

$$\pi_0^+ \to \mu_R^+ \, \nu_L \tag{1.1}$$

Applying $\hat{C}$ to this decay process gives us

$$\pi_0^- \to \mu_R^- \, \bar{\nu}_L \tag{1.2}$$

as all particles flip to their antiparticle parallels (note that this process would be forbidden as it produces a left-handed antineutrino); applying $\hat{P}$ gives us

$$\pi_0^- \to \mu_L^- \, \bar{\nu}_R \tag{1.3}$$

as particle handedness reverses (producing an allowed process of antipion decay); applying $\hat{T}$ gives us

$$\mu_L^- \, \bar{\nu}_R \to \pi_0^-. \tag{1.4}$$

We have derived the production of a pion!

But it would be too easy (and much less interesting) if the story ended there. CPT symmetry is perhaps unsatisfying in that it is only the joint $\hat{C}\hat{P}\hat{T}$ operator that is guaranteed to preserve allowability of a Standard Model process. There is no such requirement on the individual operators: in fact, we know that parity is violated in weak interactions from experiments with

Cobalt-60 (first documented in in Ref. [1]), and CP violation has been seen time and time again in the Kaon sector (first in Ref. [2]).

But the problem is even worse than that. There is a slew of evidence that the Standard Model is incomplete: neutrino oscillations imply that the particles are massive, dark matter can not be explained within the Standard Model, and most recently, experimental results from the LHCb called lepton flavour universality into question [3]. Perhaps our desire to craft an all-encompassing theory of physics that was perfectly symmetric has set us on the wrong path! We need a new theory of physics that can account for these experimental findings. And it is not unreasonable to consider new theories that allow for CPT violation: recent studies have searched for such experimental signatures in all sectors, such as in neutrino oscillations [4, 5], muon magnetic moment measurements [6], positronium emissions [7, 8], quark-antiquark mass differences [9], kaon decays [10, 11], and observations of high-redshift galaxies [12].

1.1 The Standard Model Extension

Before delving into BSM hypotheses, it is useful to briefly consider why the Standard Model should conserve CPT in the first place. This property routes back to the CPT Theorem, proved in 1954 by Luders and Pauli [13, 14]. Colloquially, the theorem states that "any Lorentz-invariant field theory describing point particles must be CPT invariant" [15]. We know that the Standard Model was constructed to be Lorentz-invariant, and Quantum Field Theory is constructed to describe point particles, so CPT conservation follows.

A sort of converse to this theorem is demonstrated in one new class of theories of physics. The Standard Model Extension (SME) was proposed in 1998 by Don Colladay and Alan Kostelecký in Ref. [16] as the most general extension to the Standard Model with a mechanism for Lorentz violation[2]; with that property comes the capacity to break CPT invariance. The mathematical formulation of the SME itself is simple: the theory consists of a set of scalars that should be added to the Standard Model Lagrangian of all orders, each term associated with a Lorentz-violating coupling. We will focus on the minimal Standard Model Extension (mSME) which includes only renormalizable terms (i.e. those with a mass dimension of four of less).

As an introduction to the mSME, we can consider the lepton sector. The Standard Model Lagrangian for leptons contains the terms

[2]The mathematical framework behind spontaneous-CPT-violating models of physics was articulated two years earlier by Colladay and Kostelecký in Ref. [17].

$$\mathcal{L}^{\text{SM}}_{\text{lepton}} \supset \frac{1}{2} i \overline{L}_A \gamma^\mu \overleftrightarrow{D}_\mu L_A + \frac{1}{2} i \overline{R}_A \gamma^\mu \overleftrightarrow{D}_\mu R_A. \tag{1.5}$$

To add in mSME physics, we need to consider CPT-even and CPT-odd terms:

$$\mathcal{L}^{\text{mSME, CPT-even}}_{\text{lepton}} \supset \frac{1}{2} i (c_L)_{\mu\nu AB} \overline{L}_A \gamma^\mu \overleftrightarrow{D}_\nu L_A + \frac{1}{2} i (c_R)_{\mu\nu AB} \overline{R}_A \gamma^\mu \overleftrightarrow{D}_\mu R_A. \tag{1.6}$$

and

$$\mathcal{L}^{\text{mSME, CPT-odd}}_{\text{lepton}} \supset - (a_L)_{\mu AB} \overline{L}_A \gamma^\mu L_A - (a_R)_{\mu\nu AB} \overline{R}_A \gamma^\mu R_A. \tag{1.7}$$

These mSME additions contain couplings with Lorentz indices $(c_{(L,R)})_{\mu\nu AB}$ and $(a_{(L,R)})_{\mu AB}$, which represent background tensors that permeate all of spacetime. Note that the full mSME Lagrangian terms are scalars, meaning that the universe as a whole does not break Lorentz symmetry: physical processes, when transformed with the background tensors, conserve this symmetry. This condition is necessary to have the mSME be compatible with General Relativity.

However, when scientists on Earth run experiments, they do so with respect to the SME background tensors. Any time, space, angle, or Lorentz transformation of an experimentalist and his apparatus means a transformation into a new background tensor value, leading to new apparent physics; to the experimentalist, Lorentz symmetry would appear to be violated[3].

Current experimental limits on the values of these background tensors in all domains of the Standard Model are documented in Ref. [18]. Searches for limits on these couplings span nearly all domains of physics, from heavy-atom interferometry to torsion pendulums to observations of binary pulsars.

For the remainder of this report, we will not make use of the full CPT violation afforded by the mSME but instead narrow ourselves to searches for *parity violation*. This choice is motivated by a desire to explore the utility of a set of *parity variables* (first presented in Ref. [19]) formulated for use on hadron collisions. This amounts to a search for nonstandard sources of parity violation at the LHC[4]. In Chap. 2, we will describe how we might use this set of variables

[3] In the context of the SME, we would say that *observer* Lorentz symmetry is conserved, while *particle* Lorentz symmetry is broken.

[4] It can be argued that a study of parity violation could be more easily done on lepton collisions (which have cleaner initial-state parity), perhaps with LEP data. There are three reasons to not do so. The first is that one of the motivations for constructing the parity variables was to gauge parity violation in "messy" hadron collisions where the parity of the initial state is not known. This is reiterated in Chap. 2. The second is that the COM

to flag for the parity violating signals at the LHC we would expect to see from mSME physics effects. The variables' utility is tested on the "Two spoons and a fork" (Sp^2F) model. The parity variables and the Sp^2F model derives from former work of the project supervisor. The coding of the Sp^2F event generator and the creation of all plots in Chap. 2 are the work of the student.

In Chap. 3, we will delve into the mathematics of the quark-sector mSME and derive Feynman rules for new parity-violating processes. All mathematical derivations are the work of the student.

In Chap. 4, we will use these Feynman rules to simulate proton-proton collisions with mSME physics effects and gauge the types of BSM experimental signals we might expect to see in the parity variables. The coding of the event generator used in Chap. 4.1 and the determination of the structure of the associated matrix element (given in Eq. (4.1)) is the joint work of the supervisor and student. The coding of the event generator used in Chap. 4.2 is the work of the student. The determination of which areas of the $c_{\mu\nu}$ and $(c_{Q,U,D})_{\mu\nu}$ matrices coupling spaces to scan, as well as all subsequent analysis, represents the ideas of the student. All plots in Chap. 4 are done by the student.

In Chap. 5, we will discuss the limitations of these toy models and provide avenues for further studies on the parity variables.

energy of the LHC is two orders of magnitude higher than that of the LEP (~ 0.1 TeV, compared with ~ 10 TeV), which allows for a search for parity violation at a previously untested energy scale. The third reason is that the author is affiliated with the ATLAS group at Cambridge, which is a LHC experiment.

Chapter 2

A brief overview of the parity variables

We are interested in determining whether the physics given by the minimal Standard Model Extension is *chiral*, or whether it is invariant under parity inversion. We are primarily interested in collisions at the LHC (proton-proton collisions). Gauging the parity of hadron collisions is more complex than doing so for fermion collisions (e.x. in electron-positron colliders) as the initial parity of a hadron collision's mother particles cannot be known (protons, being composite particles, can not be in a spin eigenstate). It is therefore desirable to have an operational flag for parity in hadron collisions, or an observable calculated on the collision products' 4-momenta that will alert us to a parity violating process.

The solution to this problem lies in a complete set of *parity variables*, denoted as V_i, defined in Ref. [19]. The authors of this paper show that for a $2 \to 2$ collision process[1], one can construct a set of 3 pseudoscalars that covers the collision space. These variables are complex algebraic functions of the 4-momenta of the mother and daughter particles for a given collision. Concretely, the variables are given by

$$\begin{aligned} V_1 &= \epsilon^{ab}_{pq} g^{a-b}_{p-q} \\ V_2 &= \epsilon^{ab}_{pq} \Re[(\Delta m^2_{a,b} + i u_1 g^{a-b}_{a+b})(\Delta m^2_{p,q} + i u_2 g^{a+b}_{p-q})] \\ V_3 &= \epsilon^{ab}_{pq} \Im[(\Delta m^2_{a,b} + i u_1 g^{a-b}_{a+b})(\Delta m^2_{p,q} + i u_2 g^{a+b}_{p-q})] \end{aligned} \tag{2.1}$$

where p, q represent mother particle 4-momenta; a, b represent daughter particle 4-momenta; u_1

[1] Technically defined as $pq \to abX$, with two daughter particles "of interest" and other decay products X. The presence of these decay products is necessary to have parity violation: a true $2 \to 2$ collision could never violate parity as it takes place entirely in one plane.

and u_2 are arbitrary constants used to ensure "dimensional self-consistency" (and are typically set to unity); ϵ^{ab}_{pq} is the determinant of a 4×4 matrix with rows p, q, a, b; $\Delta m^2_{x,y} = m^2_x - m^2_y$ is the difference between the squared masses of the particles with 4-momenta given by x, y; and g^x_y represents the 4×4 Gram determinant $G \begin{pmatrix} x, p+q \\ y, p+q \end{pmatrix}$ with

$$G \begin{pmatrix} p_1, ..., p_n \\ q_1, ..., q_n \end{pmatrix} = \begin{vmatrix} p_1 \cdot q_1 & ... & p_1 \cdot q_n \\ ... & ... & ... \\ p_n \cdot q_1 & ... & p_n \cdot q_n \end{vmatrix} \tag{2.2}$$

as the $n \times n$ Gram determinant.

It is not easy to glean physical intuition from these parity variables (which the authors of Ref. [19] acknowledge): we may note that for massless collisions, V_3 goes to zero, but there is not a clear geometric picture that can be drawn for all variables. Nevertheless, if these three variables are calculated on a set of collision events and binned, at least one of the parity variables' histograms will be asymmetric if the underlying physics of the collision events is chiral. Ref. [19] also shows that for a $2 \to 3$ collision process[2], there exists an analogous set of 19 pseudoscalars (we will not present the explicit forms for this set of variables in this report).

Given a set of collision events obeying the same physics, we can quantify the asymmetry of each of the parity variables' histograms through the following observable:

$$\Delta_{V_i} = (\#\text{ counts for } V_i < 0) - (\#\text{ counts for } V_i > 0). \tag{2.3}$$

In essence, we are creating a 3-bin histogram: positive, negative, and zero.

For the remainder of this report, we will focus on the $2 \to 3$ collision case (more specifically, $pp \to jjj$). This allows us to discard variables V_3, V_{10}, and V_{11} which go to zero when the parent particles have the same mass. As a further simplification, we assume that our daughter particles are not jets, but rather hard process quarks and gluons before hadronisation. We also assume that all particles involved in the collision are massless. This allows us to drop variables V_7, V_{12}, V_{13}, V_{16}, V_{17}, V_{18}, and V_{19}. Therefore, we consider only the nine variables V_1, V_2, V_4, V_5, V_6, V_8, V_9, V_{14}, and V_{15} (defined explicitly in Ref. [19]).

[2]Technically $pq \to abcX$.

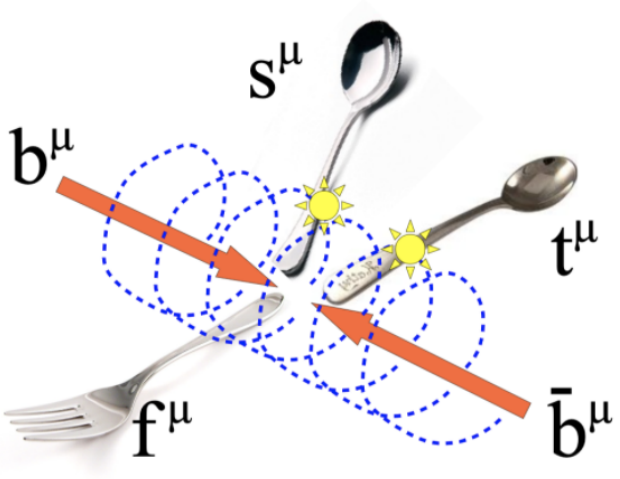

Figure 2-1: A schematic of the "Two spoons and a fork" model. The mother particles have 4-momenta b^μ and $\bar{b}^\mu$. Two daughter particles s^μ and t^μ are generated on a right-handed helix about the beam axis, and a third daughter particle f^μ conserves momentum.

2.1 Explicit parity violation: The "Two spoons and a fork" model

As a first exploration of the usefulness of the parity variables, we will calculate the variables on a system that has been engineered to violate parity: the "Two spoons and a fork" (Sp^2F) model. The Sp^2F model is an especially clean one as the parity of the system is dependent on a single parameter α.

We generate events that obey Sp^2F physics by defining a right-handed helix with pitch α centered around the beam axis, where pitch is a measure of the height of one full helix turn. For each collision, we create two daughter particles a, b (the "spoons") with spatial momenta components that lie on the helix. We also generate a third daughter particle c (the "fork") with a 4-momentum that conserves total momentum of the system. The degree of parity violation of this system is directly dependent on the helix parameter α, so if the parity variables are working properly, they should reflect this dependence. We rotate the three daughter particles about the beam axis by a random angle θ so as to avoid introducing a hard-coded anisotropy into the system, then calculate the parity variables on the daughter particles. A schematic of a Sp^2F-generating collision is shown in Fig. 2-1[3].

We scan α within the range [0.0, 0.8] GeV with a step size of 0.2 GeV[4], generating 3,000 events at each step. Each collision event is given a center-of-mass energy of 300 GeV; one

[3]Image source: C.G.Lester, private communication.

[4]The units of the pitch α are necessary so that all sinusoidal arguments in the helix equations of motion are unitless.

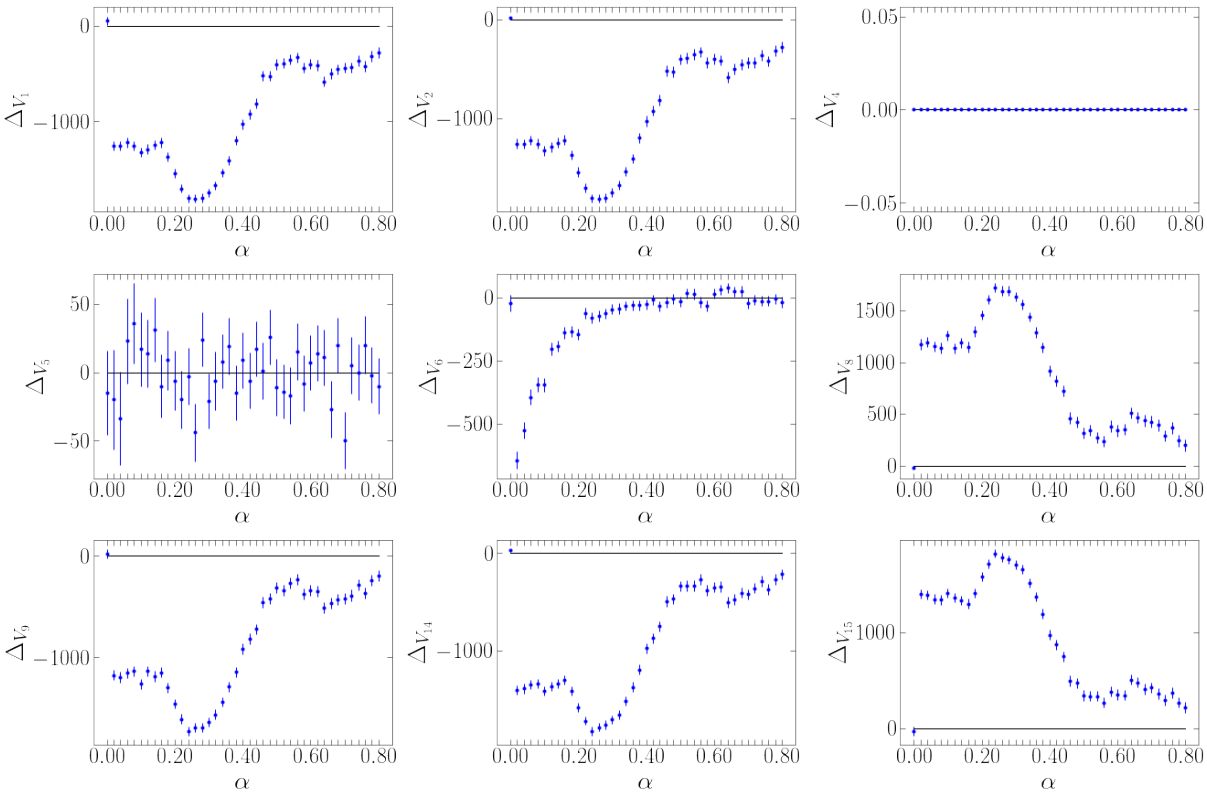

Figure 2-2: Δ_{V_i} for the Sp^2F model. Errorbars are 1σ. For $\alpha = 0$, the helix disappears and the system loses parity. The parity variables capture the simplicity of the system: six of the nine plots have the same functional form.

"spoon" daughter is generated on a helix with radius 10 GeV, and the other is generated on a helix with radius 8 GeV. We calculate the nine selected parity variables on each event, then bin the variables for a given value of α. We then calculate Δ_{V_i} and plot these values as a function of α for each Vi. Plots are shown in Fig. 2-2.

The complexity (or rather, simplicity) of the Sp^2F model is reflected in the complexity of the plots of Δ_{V_i}. Six of the nine variables show the same dependence on the single parity parameter α: the plots for V_1, V_2, V_9, and V_{14} are identical, and the plots for V_8 and V_{15} are identical to the former plots when reflected about the horizontal axis. Only V_6 shows a different dependence on α; both V_4 and V_5 show no dependence.

We have shown that the set of parity variables introduced in Ref. [19] can qualify (and, to some degree, quantify) the simple parity of the Sp^2F model. Given a clearly chiral system, the variables have flagged statistically significant parity violation, and done so in a clean manner, as shown by the shapewise similarity of the plots in Fig. 2-2. This should instill confidence in the usefulness of these parity variables for potentially more complex systems, which we will tackle in the next section.

Chapter 3

The mSME Quark Sector

Armed with a set of parity-flagging variables, we now focus on building a model of physics on which to test them. For the remainder of this report, we will focus on quark-sector physics. Our motivation for doing this is that the parity variables outlined in Chap. 2 were derived for use at the LHC (i.e. to be used on initial states without a defined parity). In this section, we will look at an alternative theory to the Standard Model that has the capability to violate parity: the Lorentz-violating minimal Standard Model Extension (mSME).

3.1 The Standard Model Quark Sector

As a warm-up, we will familiarize ourselves with the mathematical structure of the Standard Model Lagrangian. For QCD, the Lagrangian has the form

$$\mathcal{L}^{\text{SM}}_{\text{quark}} = \frac{1}{2} i \overline{Q}_A \gamma^\mu \overleftrightarrow{D}_\mu Q_A + \frac{1}{2} i \overline{U}_A \gamma^\mu \overleftrightarrow{D}_\mu U_A + \frac{1}{2} i \overline{D}_A \gamma^\mu \overleftrightarrow{D}_\mu D_A. \tag{3.1}$$

Several symbols should be defined: Q_A represents a left-handed quark doublet $\begin{pmatrix} u_A \\ d_A \end{pmatrix}_L$, U_A and D_A represent right-handed quark singlets $\Big(u_A\Big)_R$ and $\Big(d_A\Big)_R$ (respectively), capital Latin subscripts represent flavor indices, $\overleftrightarrow{D}_\mu$ represents the double-sided covariant derivative (where $A\overleftrightarrow{D}_\mu B = A(D_\mu B) - (D_\mu A)B$), and γ^μ are the standard gamma matrices.

As our aim is to look for signatures of parity violation, it will be helpful to rewrite the Standard Model Lagrangian in terms of its vector and axial interactions (a full derivation of this is given in Chap. A):

$$\mathcal{L}^{\text{SM}}_{\text{quark}} = \frac{1}{2} i\{(c_{V,u})\overline{u}\gamma^\mu \overleftrightarrow{D_\mu} u + (c_{A,u})\overline{u}\gamma^\mu \overleftrightarrow{D_\mu}\gamma^5 u + (c_{V,d})\overline{d}\gamma^\mu \overleftrightarrow{D_\mu} d + (c_{A,d})\overline{d}\gamma^\mu \overleftrightarrow{D_\mu}\gamma^5 d\}. \tag{3.2}$$

For simplicity, we restrict ourselves to two-flavour QCD and consider only interactions between up and down quarks. Here, we have replaced the chiral quark singlets and doublets with up and down spinors u and d. We have also defined four new couplings $c_{V,u}, c_{V,d}, c_{A,u}, c_{A,d}$, as

$$\begin{aligned}
(c_{V,u})_{\mu\nu} &= +(c_Q)_{\mu\nu} + (c_U)_{\mu\nu} \\
(c_{A,u})_{\mu\nu} &= -(c_Q)_{\mu\nu} + (c_U)_{\mu\nu} \\
(c_{V,d})_{\mu\nu} &= +(c_Q)_{\mu\nu} + (c_D)_{\mu\nu} \\
(c_{A,d})_{\mu\nu} &= -(c_Q)_{\mu\nu} + (c_D)_{\mu\nu}
\end{aligned} \tag{3.3}$$

The first two are couplings to the quark *vector* interactions, and the second two are couplings to the quark *axial* interactions, which are also accompanied by the γ^5 matrix. Recall that the transformation properties for a vector require that the spatial components flip sign under a parity transformation and the time component stays the same, while the reverse transformation property holds for an axial vector.

In the Standard Model, the QCD vector couplings are turned on ($c_{V,u} = c_{V,d} = 2$) and the axial couplings are turned off ($c_{A,u} = c_{A,d} = 0$). This is confirmed experimentally: no quark-sector experiments have shown any degree of parity violation.

3.2 The mSME Quark Sector

The mSME modifies quark-quark interactions by adding a CPT-even and a CPT-odd term to the Lagrangian, with

$$\mathcal{L}^{\text{CPT-even}}_{\text{quark}} = \frac{1}{2} i\{(c_Q)_{\mu\nu AB}\overline{Q}_A\gamma^\mu \overleftrightarrow{D^\nu} Q_B + (c_U)_{\mu\nu AB}\overline{U}_A\gamma^\mu \overleftrightarrow{D^\nu} U_B + (c_D)_{\mu\nu AB}\overline{D}_A\gamma^\mu \overleftrightarrow{D^\nu} D_B\} \tag{3.4}$$

and

$$\mathcal{L}^{\text{CPT-odd}}_{\text{quark}} = -\{(a_Q)_{\mu AB}\overline{Q}_A\gamma^\mu Q_B + (a_U)_{\mu AB}\overline{U}_A\gamma^\mu U_B + (a_D)_{\mu AB}\overline{D}_A\gamma^\mu D_B\}. \tag{3.5}$$

For the mSME, these $c_{\mu\nu}$ and a_μ couplings are not scalars but composite tensors that permeate

all of spacetime. It is these background tensors that lead to Lorentz, and therefore CPT, violation. We will consider parity violation that comes from combinations of parity-odd and parity even $c_{\mu\nu AB}$ terms, and leave effects due to $\mathcal{L}^{\text{CPT-odd}}_{\text{quark}}$ out of this analysis.

As before, it is helpful to rewrite the mSME Lagrangian in terms of its vector and axial interactions, shown below:

$$\begin{aligned}&\mathcal{L}^{\text{CPT-even}}_{\text{quark}} = \\ &\frac{1}{2}i\{(c_{V,u})_{\mu\nu}\overline{u}\gamma^{\mu}\overleftrightarrow{D^{\nu}}u + (c_{A,u})_{\mu\nu}\overline{u}\gamma^{\mu}\overleftrightarrow{D^{\nu}}\gamma^{5}u + (c_{V,d})_{\mu\nu}\overline{d}\gamma^{\mu}\overleftrightarrow{D^{\nu}}d + (c_{A,d})_{\mu\nu}\overline{d}\gamma^{\mu}\overleftrightarrow{D^{\nu}}\gamma^{5}d\}.\end{aligned} \tag{3.6}$$

Note that our mSME vector and axial couplings have spacetime indices, as opposed to our Standard Model couplings. The origin of these SME terms comes from the tetrad, or *vierbein*, formalism of general relativity. The tetrad, defined as

$$e^{a}{}_{\beta} = \frac{\partial \xi^{a}_{X}(x)}{\partial x^{\beta}}\Big|_{x=X}, \tag{3.7}$$

is a set of four vector fields that represent a spacetime coordinate change between global (x^{β}) and locally inertial coordinates (ξ^{a}). Its usefulness is mainly computational, as it defines the transformation laws into the inertial coordinate frame that the user deems to be the best-suited for solving a given problem.

In its full expansion, the SME would contain the vector and axial couplings

$$\begin{aligned}\mathcal{L}^{\text{CPT-even}}_{\text{quark, vector}} &= -\frac{1}{2}i(c_{V})_{\lambda\nu}ee^{\mu}{}_{a}e^{\nu a}e^{\lambda}{}_{b}\overline{\psi}\gamma^{b}\overleftrightarrow{D^{\nu}}\psi \\ \mathcal{L}^{\text{CPT-even}}_{\text{quark, axial}} &= -\frac{1}{2}i(c_{A})_{\lambda\nu}ee^{\mu}{}_{a}e^{\nu a}e^{\lambda}{}_{b}\overline{\psi}\gamma_{5}\gamma^{b}\overleftrightarrow{D^{\nu}}\psi\end{aligned} \tag{3.8}$$

where the tetrad determinant $e = \sqrt{-g}$, where $g_{\mu\nu}$ is the global metric. In Minkowski space, the vierbein collapses to $e^{a}{}_{\beta} \to \delta^{a}{}_{\beta}$. This leads to the SME Lagrangian of the form in Eq. (3.6).

Based on the partial derivative structure of the tetrads, it can be shown that couplings of the form $(c_{V,A})_{00}$ and $(c_{V,A})_{ij}$ are even under the parity operator, and couplings of the form $(c_{V,A})_{0j}$ and $(c_{V,A})_{i0}$ are odd. Parity-violating signals require the interference of both parity-odd and parity-even terms.

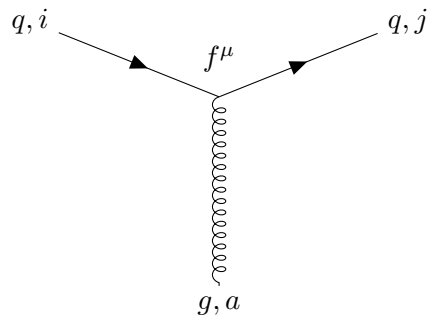

Figure 3-1: Feynman diagram for the quark-quark-gluon vertex. The diagram has a matrix element contribution of $-ig_s\frac{\lambda^a_{ij}}{2}f^\mu$. In the Standard Model, $f^\mu = \gamma^\mu$; in the mSME, this term is a more complex structure incorporating the background spacetime tensors.

3.3 Quark-quark-gluon interactions in the mSME

We would now like to derive a vertex that captures the mSME effects on quark-quark-gluon interactions, illustrated in the vertex in Fig. 3-1. We can do this by reading off the Feynman rules from Eq. (3.6), after a little more simplification. The covariant derivative should first be expanded out, revealing the gauge couplings $D_\mu = \partial_\mu - ig_s G^a_\mu \frac{\lambda_a}{2}$. Here, λ_a represents the Gell-Man matrices (where a sums over the set of eight), and G^a_μ represents the gluons.

Considering only the gauge-coupling terms from the covariant derivative and replacing the double-headed arrow in Eq. (3.6), we find

$$\begin{aligned}&\mathcal{L}^{\text{CPT-even}}_{\text{quark}} \supset \\ &g_s\frac{\lambda_a}{2}\{(c_{V,u})_{\mu\nu}\overline{u}\gamma^\mu G^{a\nu}u + (c_{A,u})_{\mu\nu}\overline{u}\gamma^\mu G^{a\nu}\gamma^5 u + (c_{V,d})_{\mu\nu}\overline{d}\gamma^\mu G^{a\nu}d + (c_{A,d})_{\mu\nu}\overline{d}\gamma^\mu G^{a\nu}\gamma^5 d\}.\end{aligned} \tag{3.9}$$

At this point, we can read off the Feynman rule. The mSME vertex should be equal to $-ig_s\gamma^\mu\frac{\lambda^a_{ij}}{2}\frac{(c_{V,q})_{\mu\nu}+(c_{A,q})_{\mu\nu}\gamma^5)}{2}$. This can be compared with the Standard Model quark-quark-gluon vertex, which is given by $-ig_s\gamma^\nu\frac{\lambda^a_{ij}}{2}\frac{(c_{V,q}+c_{A,q}\gamma^5)}{2}$ (with $c_{V,q} = 2$; again, we are assuming no flavor mixing).

In summary: the addition of the mSME to the quark sector provides us with a full vertex

$$f_\nu = -ig_s\frac{\lambda^a_{ij}}{2}(\gamma_\nu + \gamma^\mu\frac{(c_{V,q})_{\mu\nu} + (c_{A,q})_{\mu\nu}\gamma^5)}{2}). \tag{3.10}$$

By switching on certain combinations of the $(c_{V,A})_{\mu\nu}$ matrix elements, we can create parity-violating signals in the quark sector.

3.3.1 The mSME as an effective momentum transformation

It was shown in Ref. [20] that the physics of photon-mediated quark scattering could be reproduced by changing the metric from $\eta_{\mu\nu}$ to $\eta_{\mu\nu}+c_{\mu\nu}$ (see section 3.3, "Minimal c-type coefficients", [20]). In the modified Breit frame, the SME matrices can be absorbed into physical momenta with the transformation $p_\mu \to (\eta_{\mu\nu} + c_{\mu\nu})p^\nu$.

This interpretation is somewhat intuitive: we essentially have a metric transformation from flat spacetime to something more complex, governed by background tensors. Note that we have the capability to transform the momenta of different particles in different ways, so not all classes of particles experience the same local geometries. Indeed, the true mSME has different couplings for different particle flavors.

We have outlined the basics of the parity-violating quark sector of mSME, as well as introduced a more intuitive "effective transformation" version. Both of these models serve as the basis for the parity-violating toy models of physics that we will test the parity variables on in the next section. Our overall goal is to find a link between the $(c_{V,A})_{\mu\nu}$ couplings and any qualitative or quantitative signal in the parity variables for proton-protom collisions. If we were able to find such a link in simulation, then this could provide an avenue for a search for mSME effects at the LHC.

Chapter 4

Two mSME Simulations

Now that we have found a theory of physics with a mechanism for parity violation in proton-proton collisions, we can ask about the ability of the parity variables defined in Ref. [19] to catch this violation. In this chapter, we will consider two models of physics with the capacities to violate parity: the first is a more simple simulation based on the presence of a single minimal Standard Model Extension (mSME) background tensor $c_{\mu\nu}$; the second is a more faithful representation of the full mSME with three background tensors $(c_Q)_{\mu\nu}$, $(c_U)_{\mu\nu}$, and $(c_D)_{\mu\nu}$ from Eq. (3.4).

4.1 Simulation I: The toy generator

We first consider the detectable parity violation from a toy version of the mSME inspired by the effective momentum transformation outlined in Chap. 3.3.1.

We consider a massless $2 \to 3$ collision process, with mother particles p, q and daughter particles a, b, c. We associate with this process a matrix element

$$\mathcal{M} = c_{\text{odd}} \frac{\varepsilon_{\mu\nu\sigma\rho} p^\mu q^\nu a^\sigma b^\rho}{|p+q|^5 |a+b|^3} \times G\begin{pmatrix} a-b, p+q \\ p-q, p+q \end{pmatrix} + c_{\text{even}} \frac{(p\cdot q)(a\cdot b)}{(p+q)^2 (a+b)^2}. \tag{4.1}$$

where

$$G\begin{pmatrix} p_1, ..., p_n \\ q_1, ..., q_n \end{pmatrix} = \begin{vmatrix} p_1\cdot q_1 & ... & p_1\cdot q_n \\ ... & ... & ... \\ p_n\cdot q_1 & ... & p_n\cdot q_n \end{vmatrix} \tag{4.2}$$

is a $n \times n$ Gram determinant.

This matrix element has been chosen as the sum of the simplest parity-odd and parity-

even quantities that could be constructed from the mother and daughter 4-momenta that are invariant with respect to exchanges of p and q, and of a and b[1]. Denominators are set to make the matrix unitless.

To simulate mSME physics, we apply the effective momentum transformation $k_\mu \to c_{\nu\mu}k^\nu$ to various parts of the matrix element given in Eq. (4.1). We consider two categories of transformations:

1. `sim`: The momentum transformation is applied simultaneously to daughter momenta a and b.

2. `sum`: The momentum transformation is applied separately to daughter particles a and b, giving two matrix elements $\mathcal{M}_{\texttt{just\_a}}$ and $\mathcal{M}_{\texttt{just\_b}}$. We then take the average of these elements. Such a term might come from an interference term between the Standard Model vertex being applied to one daughter particle and the mSME qqg vertex component being applied to the other.

4.1.1 Event generation

Event generation for the "effective momentum transformation" model is a three part process.

1. *Set the physics.* Choose a value of the momentum transformation $c_{\mu\nu}$ matrix. In order to make plots that can be visualized on a two-dimensional surface, it is necessary to use sparse $c_{\mu\nu}$ matrices each with two degrees of freedom. In this analysis, we consider two classes of matrices: (1) diagonal and (2) mixed, described in more detail in Chap. 4.1.2.

2. *Generate the collision events.* Generate 5,000 $2 \to 3$ collisions. Set the 4-momenta of the two mother particles to be $p^\mu = (1, 0, 0, 1)$ and $q^\mu = (1, 0, 0, -1)$, and generate 3 massless daughter particles with random energies and angles uniformly distributed on a sphere.[2] For each collision, numerically calculate the squared matrix element $|\mathcal{M}|^2$ as defined in Eq. (4.1), after applying one of the predefined momentum transformations. Use this as the event weight.

3. *Evaluate the parity variables asymmetry.* For each of the nine parity variables, calculate the quantity Δ_{V_i}, as defined in Eq. (2.3). (Note that the parity variables are calculated on the untransformed daughter momenta.)

[1] For proton-proton collisions that produce three jets at the LHC, we would likely have no way of distinguishing between the initial protons, or between any of the daughter jets.

[2] To circumvent collider singularities, we also ensure that the daughter particles are all separated from each other and the beam axis by $R = 0.1$ radians.

4.1.2 Results

Here we present the results of the two-dimensional scans for the diagonal and mixed $c_{\mu\nu}$ matrix cases. In all cases, both variables are scanned over the interval $[-1.05, 1.05]$ with a gradation of 0.15.

(1) Diagonal scan

For this class of scans, we choose a diagonal transformation matrix $c_{\mu\nu}$. For each setup, we pick two of the diagonal elements to scan over. The other two diagonal elements are set to be equal to each other and to make the full $c_{\mu\nu}$ matrix traceless. We consider every combination of diagonal scans: (c_{00}, c_{11}), (c_{00}, c_{22}), (c_{00}, c_{33}), (c_{11}, c_{22}), (c_{11}, c_{33}), (c_{22}, c_{33}).

The resulting plots can be categorized into five types of trends, shown in Fig. 4-1 and described below:

1. *Flipper*, shown in Fig. 4-1a. These plots show the most significant parity violation when the two scan variables are equal in sign and largest in magnitude. There is a sharp change in sign of the Δ_{V_i} functions across the main diagonal.

   - Relevant scans: `sim` c_{00}, c_{11}; `sim` c_{00}, c_{22}; `sim` c_{00}, c_{33}

2. *Tight double headed arrow*, shown in Fig. 4-1b. These plots show the most significant parity violation when the two scan variables are equal in sign and largest in magnitude. In contrast to the previous class, these plots show a change in sign of the Δ_{V_i} functions when the sign of both scan variables changes.

   - Relevant scans: `sim` c_{11}, c_{22}; `sim` c_{11}, c_{33}; `sim` c_{22}, c_{33}

3. *Single headed arrow*, shown in Fig. 4-1c. These plots only show their chirality when both scan variables are positive **or** negative.

   - Relevant scans: `sum` c_{00}, c_{33}; `sum` c_{11}, c_{22}

4. *Loose double headed arrow*, shown in Fig. 4-1d. These plots are like the *tight double headed arrow* ones, but are much more diffuse.

   - Relevant scans: `sum` c_{00}, c_{11}; `sum` c_{00}, c_{22}

5. *No trend*, shown in Fig. 4-1e.

   - Relevant scans: `sum` c_{11}, c_{33}; `sum` c_{22}, c_{33}

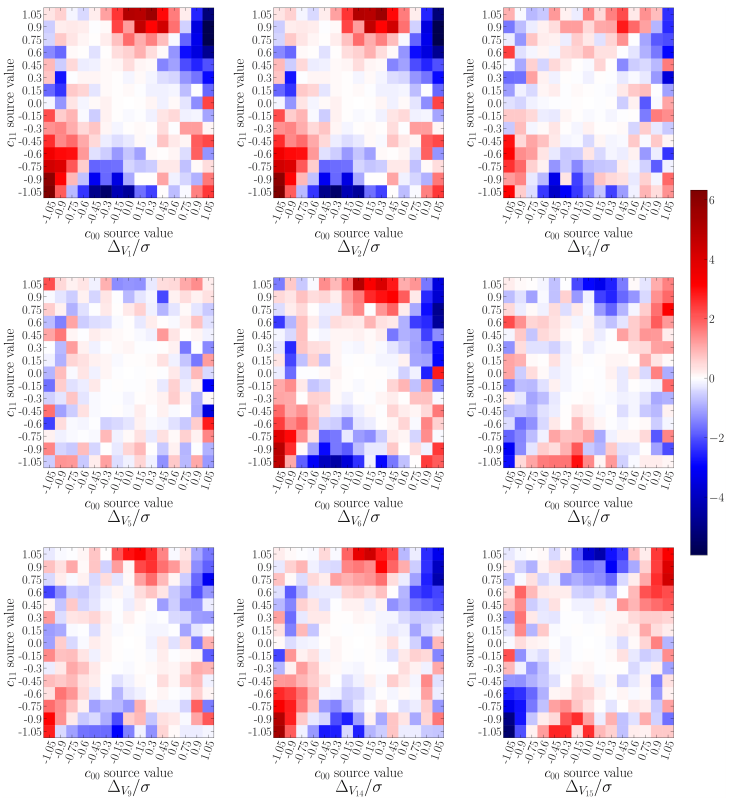

(a) Δ_{V_i}/σ for *flipper* trend, shown for `sim` with scan variables c_{00} and c_{11}

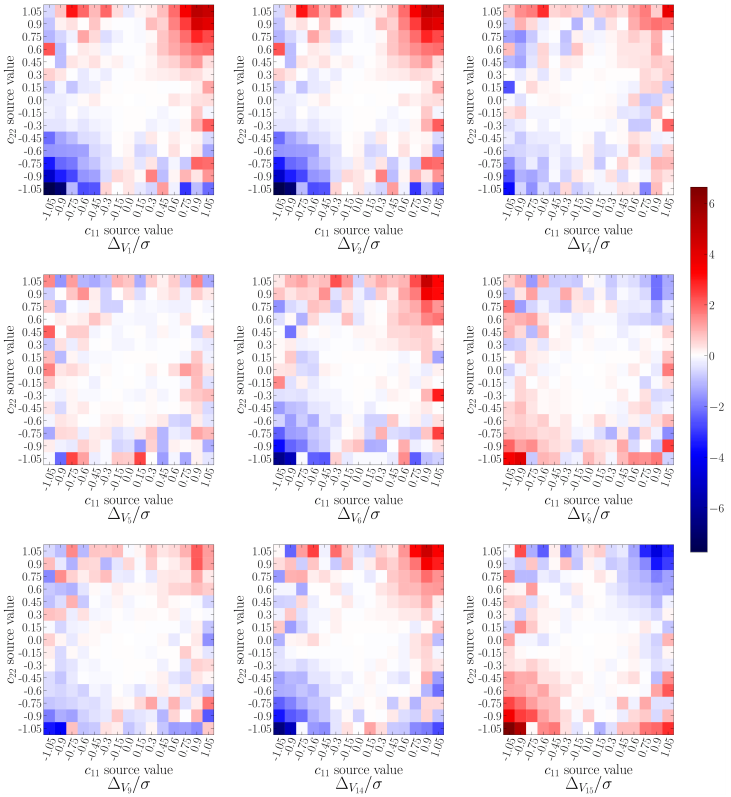

(b) Δ_{V_i}/σ for *tight double headed arrow* trend, shown for `sim` with scan variables c_{11} and c_{22}

Figure 4-1: Diagonal scan results (1/3)

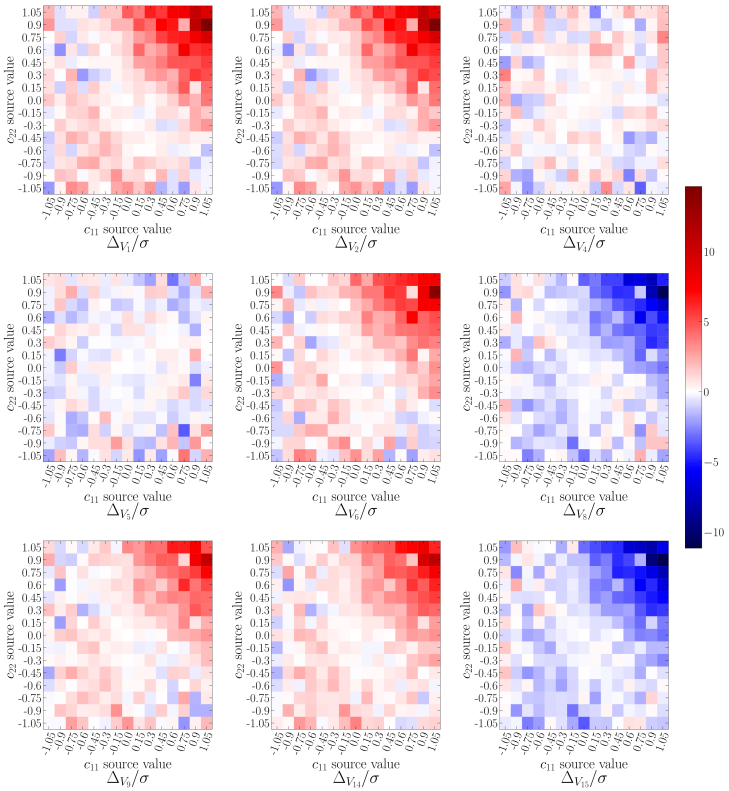

(c) Δ_{V_i}/σ for *single headed arrow*, shown for `sum` with scan variables c_{11} and c_{22}

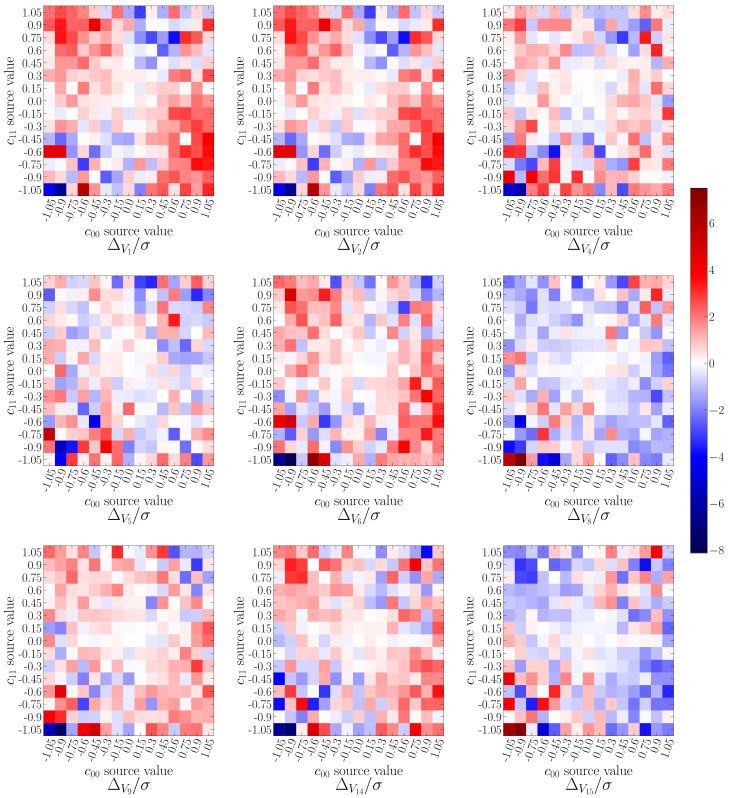

(d) Δ_{V_i}/σ for *loose double headed arrow*, shown for `sum` with scan variables c_{00} and c_{11}

Figure 4-1: Diagonal scan results (2/3)

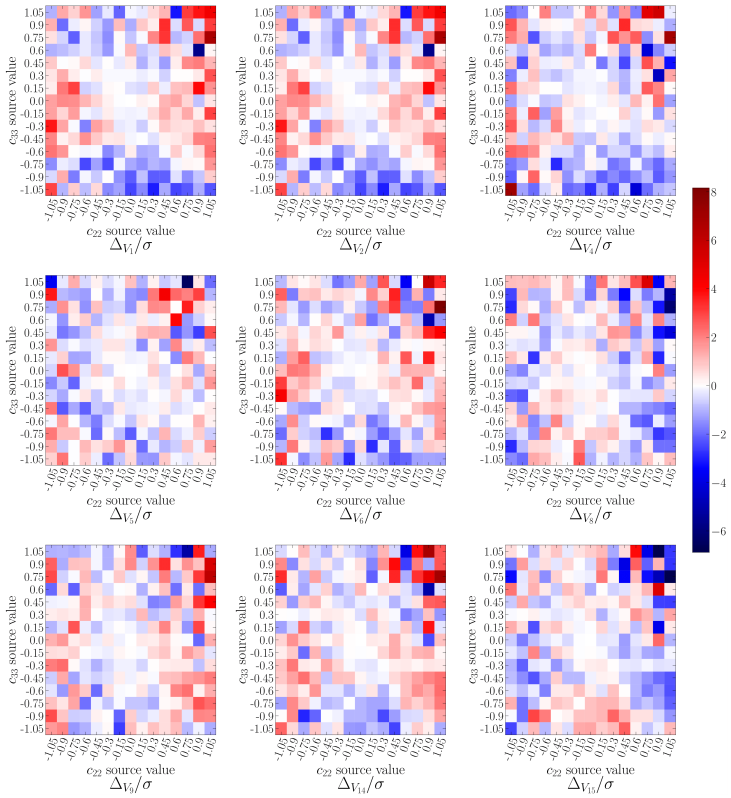

(e) Δ_{V_i}/σ for *no trend*, shown for `sum` with scan variables c_{22} and c_{33}

Figure 4-1: Diagonal scan results (3/3)

In general, we do see trending in the parity variables as we scan over the diagonal matrix elements of $c_{\mu\nu}$. Variables V_1, V_2, V_8, V_9, V_{14}, and V_{15} seem to be the most responsive, although V_4 and V_9 do show some trending. There is redundancy in the variables as well: the plots for V_1 and V_2 are identical, and the plots for V_8 and V_9, and V_{14} and V_{15}, are additive inverses.

Comfortingly, the space directions x and y are treated on equal footing (e.x. plots of scans over c_{00} and c_{11} closely resemble those of scans over c_{00} and c_{22}). This is logical, considering the symmetry in ϕ at the LHC.

For the vast majority of the plots (except the *single headed arrow* case), the strength of the parity violation increases with the size of the $c_{\mu\nu}$ coefficients, which we would expect, as the coefficients also change the magnitude of the transformed momenta and therefore the matrix element. Plots generated with `sim` physics seem to be "tighter" than those generated with `sum` plots (compare Fig. 4-1b and Fig. 4-1d for an example of this), which might also be expected: the `sum` generations contain one term with two transformed momenta, while the `sim` generations contain two terms each with one transformed momentum. It is likely that the *no trend* cases are those where the $c_{\mu\nu}$ transformations lead to no change in the relative sizes of the parity-odd and parity-even part of the matrix element given in Eq. (4.1).

(2) Mixed scan

For each setup in our mixed scan case, we choose one c_{0i} and one c_{ij} element to scan over, with $i \neq j$. For each real scan value α, we set the matrix element to be $\alpha(1+i)$. As the $c_{\mu\nu}$ matrices are Hermitian, we must also turn on c_{i0} and c_{ji}. We consider every combination of diagonal scans: (c_{01}, c_{12}), (c_{01}, c_{13}), (c_{02}, c_{21}), (c_{02}, c_{23}), (c_{03}, c_{31}), (c_{03}, c_{32}).

The mixed scan cases show some trending in the parity variables, but not nearly to the same degree of tightness as was present in the diagonal scan cases – in fact, there is no observable trending for any of the `sim` cases. We do see the same pairwise relations between V_1 and V_2, V_8 and V_9, and V_{14} and V_{15}. In addition, the x and y directions are treated on equal footing.

The two types of trends are shown in Fig. 4-2, and are described below.

1. *Overall trend*, shown in Fig. 4-2a. These plots do not show parity violation within a variable, but rather across: note the change in overall plot sign from V_8 to V_9, and V_{14} to V_{15}.

    - Relevant scans: all `sum` cases

2. *No trend*, shown in Fig. 4-2b.

    - Relevant scans: all `sim` cases

The results for the mixed scan generations are significantly less nuanced than those for the diagonal scan generations. This could be due to there being fewer degrees of freedom in the mixed scans. While both scans have two independent scan variables (necessary to make two-dimensional plots), the diagonal scan cases contain a third "meaningful" number: recall that the $c_{\mu\nu}$ matrices should be traceless, so the two non-scan diagonal elements were set to be nonzero to fit this constraint. However, the mixed scan cases did not have this constraint, and contained no information other than the two dependent scan variables.

As an overall conclusion to our first toy mSME model: if the toy model were not leading to any parity-violating physics, we would expect our variables Δ_{V_i} to increase in magnitude as the $c_{\mu\nu}$ coefficients increased, simply due to both the parity-odd and parity-even components of Eq. (4.1) increasing in tandem. In fact, we do see these results in the *no trend* plots. However, all of the non *no trend* plots contain signals in the parity variables that are linked to certain combinations of $c_{\mu\nu}$ coefficients being turned on, rather than their magnitude (perhaps the best example of this is the *single headed arrow* trend). We can thus conclude with some confidence that the mSME effective transformation is producing chiral physics, and that the parity variables can detect it.

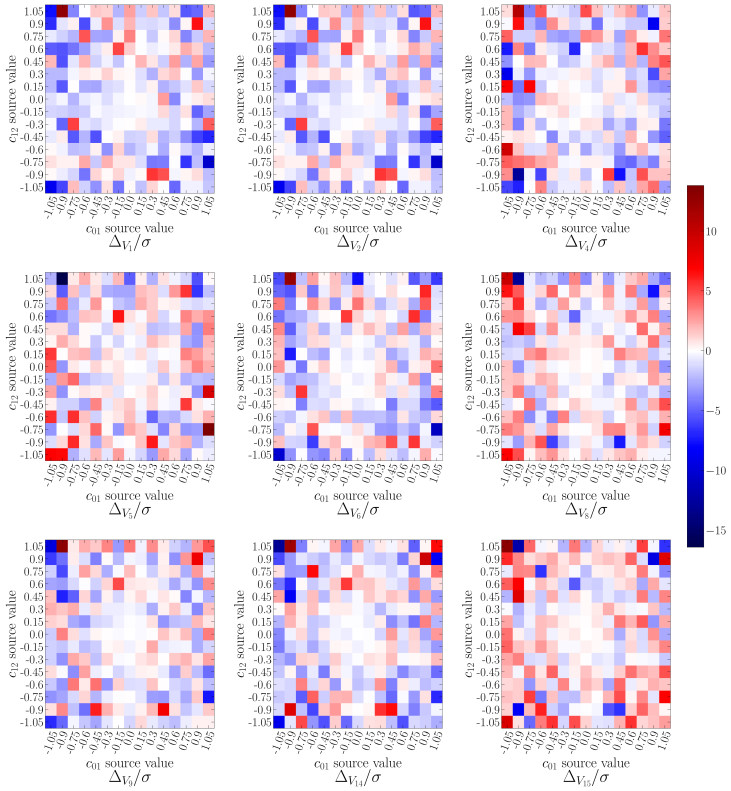

(a) Δ_{V_i}/σ for *overall trend*, shown for `sum` with scan variables c_{01} and c_{12}

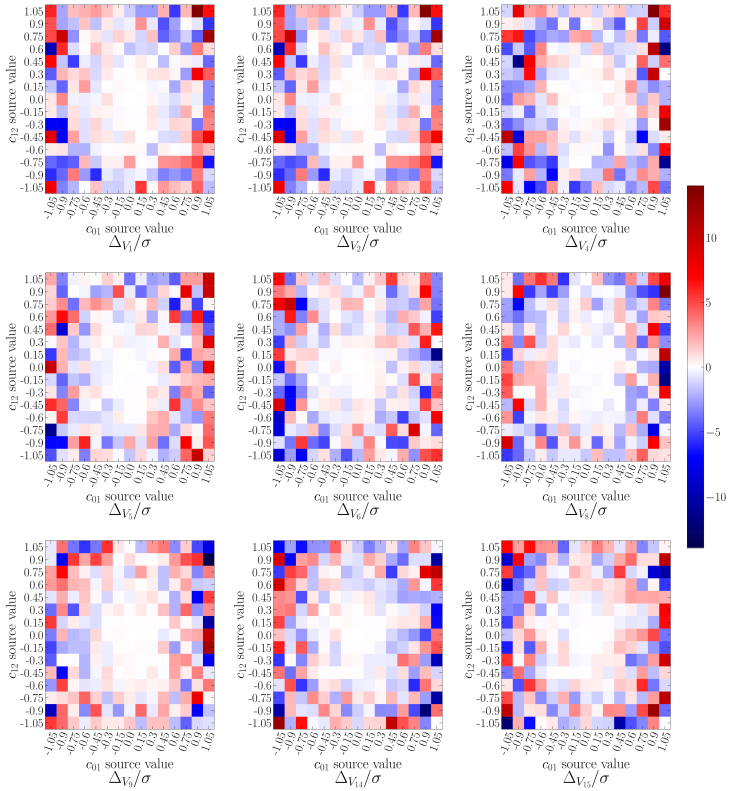

(b) Δ_{V_i}/σ for *no trend*, shown for `sim` with scan variables c_{01} and c_{12}

Figure 4-2: Mixed scan results (1/1)

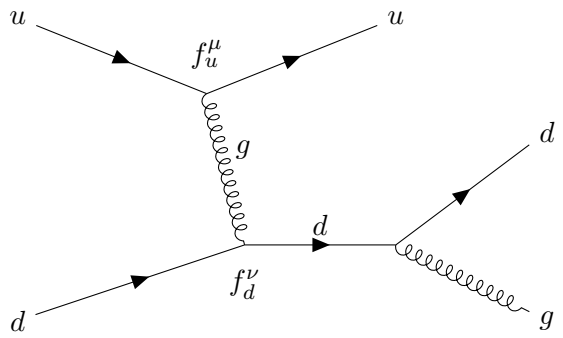

Figure 4-3: Feynman diagram for the process $ud \to udg$. Vertices f_u^μ and f_d^ν are defined in Eq. (4.3) and include SME couplings. For computational simplicity, we have assumed that the rightmost ddg vertex contains no SME effects.

4.2 Simulation II: Single diagram mSME physics

For our final simulated physics model, we consider a single quark-sector SME matrix element corresponding to a $2 \to 3$ collision $ud \to udg$. The associated Feynman diagram is shown in Fig. 4-3, and it has a matrix element of

$$|\mathcal{M}|^2 = \overline{u}(p_3) f_u^\mu u(p_1) \frac{-i\eta_{\mu\nu}}{(p_3 - p_1)^2} \overline{u}(p_4) \gamma^\alpha \epsilon_\alpha^* \frac{i(p_4 + p_5)_\beta \gamma^\beta}{(p_4 + p_5)^2} f_d^\nu u(p_2) \tag{4.3}$$

where p_1 and p_3 are the 4-momenta of the incoming and outgoing up quarks, p_2 and p_4 are the 4-momenta of the incoming and outgoing down quarks, and p_5 is the 4-momentum of the outgoing gluon. The two vertices f_u^μ and f_d^ν are the Standard Model + mSME vertices for the up and down quarks, respectively; in long form, they are equal to

$$\begin{aligned} f_u^\mu &= \gamma^\mu + \frac{1}{2}\gamma_\pi((c_{V,u})^{\pi\mu} + (c_{A,u})^{\pi\mu}\gamma^5) \\ f_d^\nu &= \gamma^\nu + \frac{1}{2}\gamma_\pi((c_{V,d})^{\pi\nu} + (c_{A,d})^{\pi\mu}\gamma^5). \end{aligned} \tag{4.4}$$

4.2.1 Event Generation

Event generation for this toy model is more complex than for the proceeding one, as the total available coupling space is 45-dimensional. The couplings are derived from the three 4-by-4 matrices $(c_Q)_{\mu\nu}$, $(c_U)_{\mu\nu}$, and $(c_D)_{\mu\nu}$ from Eq. (3.4), each of which is a complex traceless Hermitian matrix with 15 degrees of freedom. Our preliminary studies showed that lighting up only two $(c_{Q,U,D})_{\mu\nu}$ matrix elements at a time would be unlikely to produce detectable parity violation. We therefore probe this couplings space with a bogosearch. For each run, we randomly generate the three couplings matrices, populating all 45 dimensions. We use these matrices to calculate the vector and axial coupling matrices for the up and down quarks $(c_{V,u})_{\mu\nu}$,

$(c_{A,u})_{\mu\nu}$, $(c_{V,d})_{\mu\nu}$, and $(c_{A,d})_{\mu\nu}$.

Calculation of the matrix element is done numerically. The generation process is as follows:

1. *Set the physics.* Randomly generate the three Hermitian matrices $(c_Q)_{\mu\nu}$, $(c_U)_{\mu\nu}$, and $(c_D)_{\mu\nu}$. Calculate the 4 Hermitian matrices $(c_{V,u})_{\mu\nu}$, $(c_{A,u})_{\mu\nu}$, $(c_{V,d})_{\mu\nu}$, and $(c_{A,d})_{\mu\nu}$ using Eq. (3.3).

2. *Survey the phase space.* Generate 5,000 $2 \to 3$ collisions. Set the 4-momenta of the two mother particles to be $p^\mu = (1, 0, 0, 1)$ and $q^\mu = (1, 0, 0, -1)$, and generate three massless daughter particles with random energies and angles uniformly distributed on a sphere. For each collision, numerically calculate the squared matrix element $|\mathcal{M}|^2$ as defined in Eq. (4.3), and make a note of the maximum value $|\mathcal{M}|^2_{\max}$. This value, multiplied by 10, will be treated as the theoretical maximum squared matrix element for the process.

3. *Generate the collision events.* Generate 10,000 $2 \to 3$ collisions as before. For each collision, calculate and store the nine nonzero parity variables and an event weight $\frac{|\mathcal{M}|^2}{10\times|\mathcal{M}|^2_{\max}}$.

4. *Evaluate the parity variables asymmetry.* For each of the nine parity variables, calculate the quantity Δ_{V_i}, as defined in Eq. (2.3).

To summarize: for each random instantiation of the matrices $(c_Q)_{\mu\nu}$, $(c_U)_{\mu\nu}$, and $(c_D)_{\mu\nu}$, we can calculate nine numbers Δ_{V_i} (and their error) which can be used to gauge the chirality of the mSME physics. We repeat the aforementioned steps for a large number (n = 1,000) of mSME matrix instantiations.

4.2.2 Results

Fig. 4-4 shows Δ_{V_i} for each variable over all 1,000 mSME matrix instantiations. Most random generations do not produce significantly chiral physics; however, there are some instantiations that produce deviations from zero that are significant to over 3σ.

Assuming a Gaussian distribution, we expect 1% of the total instantiations to be significant to over 3σ without coming from an underlying signal. We are therefore looking for an excess of 10 "hits" outside of the 3σ regions in Fig. 4-4. For most variables, this excess is present (though not to a large degree – the excess is usually on the order of 10 as well). In Fig. 4-5, we histogram the Δ_{V_i}/σ data contained in Fig. 4-4 and fit a Gaussian curve to the distributions, finding again an excess of hits on the tails of the Gaussian. This implies that some of the $(c_{Q,U,D})_{\mu\nu}$ matrix instantiations are able to make statistically significant parity-violating physics.

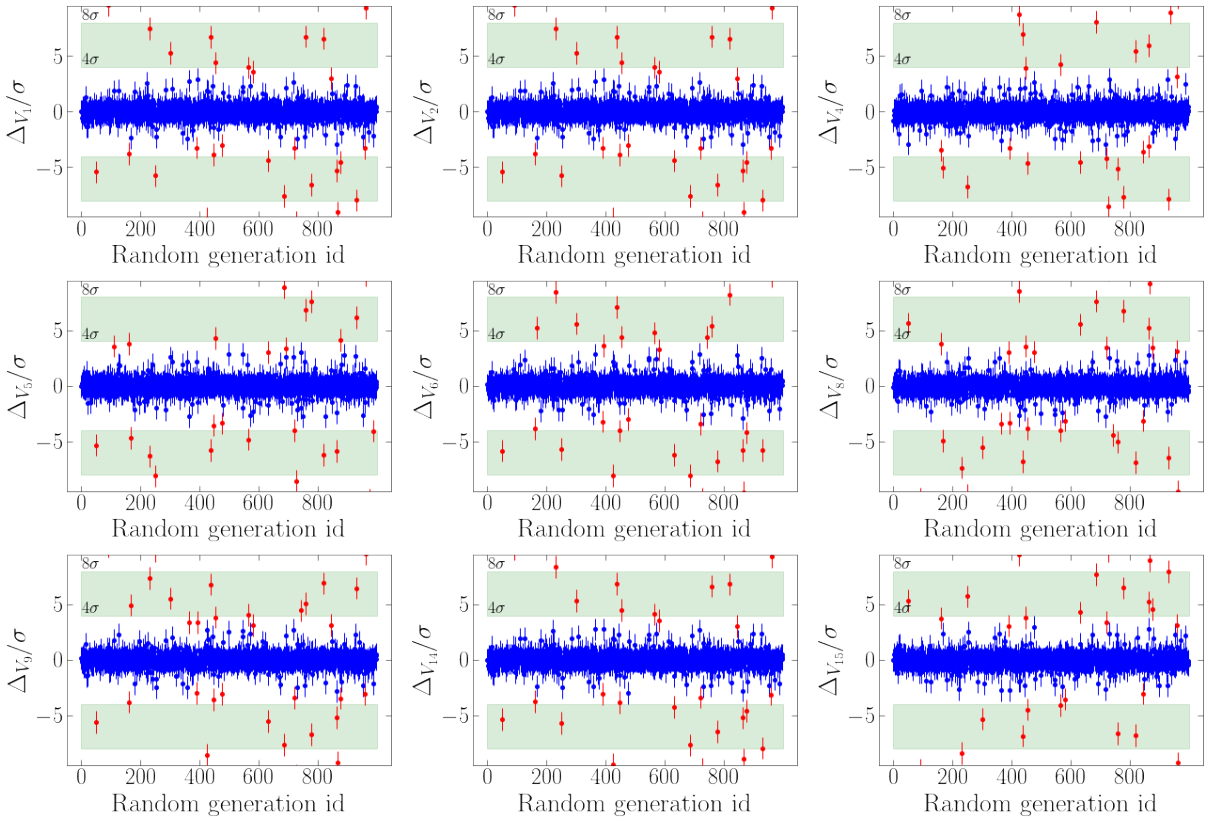

Figure 4-4: Δ_{V_i}/σ for all 1,000 instantiations of the $(c_{Q,U,D})_{\mu\nu}$ matrices. Errorbars are for 1σ. Instantiations outside of the 3σ line are shown in red. Bands representing anomalies between (4-8)σ have been highlighted in green; these bands select mSME instantiations that will be used in Chap. 4.2.3.

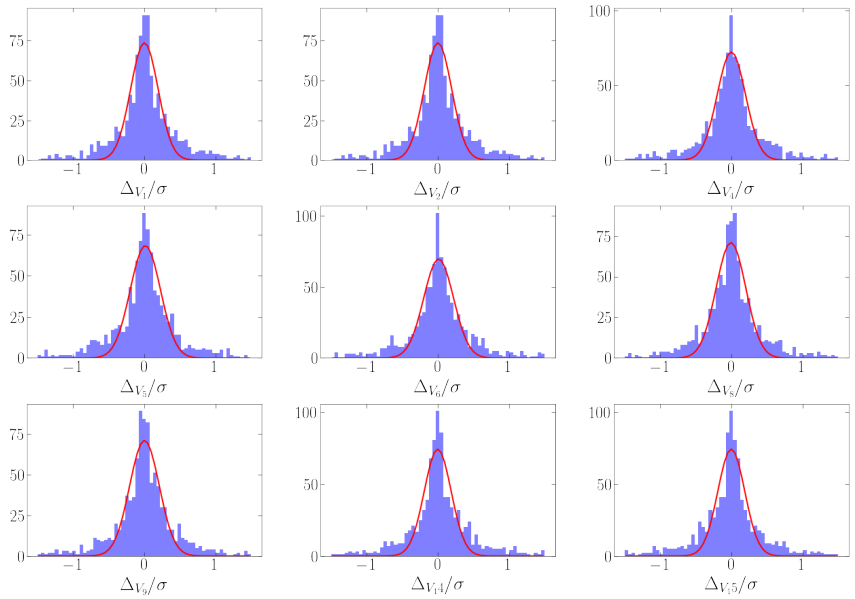

Figure 4-5: Histograms of Δ_{V_i}/σ for all 1,000 random instantiations of the $(c_{Q,U,D})_{\mu\nu}$ matrices, plotted with a Gaussian fit. The excess in hits on the tails of the Gaussian could be evidence of parity-violating instantiations.

4.2.3 Reproducibility studies

From Fig. 4-4, we can see that for a given parity variable, there are a few $(c_{Q,U,D})_{\mu\nu}$ matrix instantiations that seem to produce significantly chiral physics (i.e. $\Delta_{V_i} \neq 0$ to greater than 3σ). To gauge whether this chirality is genuine (rather than a random fluke of the kinematic event generation), we need to make sure that it is reproducible. In other words, $(c_{Q,U,D})_{\mu\nu}$ setups that are truly parity violating in V_i should produce significantly nonchiral physics in V_i when the kinematic simulation is rerun with different random seeds.

To test for parity reproducibility, we follow the steps below:

1. *Set the physics.* For a given variable V_i, average over all instantiations where Δ_{V_i} is significantly positive (or negative) to between than (4-8)σ. An example averaged matrix setup for V_1 anomalies is shown in Fig. 4-6.

2. *Generate repeatedly.* Generate 10,000 collision events 50 times, each time with the same $(c_{Q,U,D})_{\mu\nu}$ matrices set and with a different random seed.

3. *Evaluate the parity variables asymmetry.* For each of the 50 trials, evaluate the quantity Δ_{V_i} and its error.

Results are shown in Fig. 4-7 (averaging over all $(c_{Q,U,D})_{\mu\nu}$ setups with Δ_{V_i} significantly positive) and Fig. 4-7(with Δ_{V_i} significantly negative). For 50 random seems runs, we would expect 0 to 1 run to be statistically significant to over 3σ due to Gaussian fluctuations. Unfortunately, no plot showed convincing evidence of a continuously parity-violating signal (i.e. a large number of statistically significant hits). The closest signal of parity violation is seen in the positive $\Delta_{V_{14}}$ plot, which has 5 hits that are just shy of being anomalous to 3σ. However, this signal in isolation might easily be attributed to the look-elsewhere effect. Evidently, the chirality found in the initial surveys of the $(c_{Q,U,D})_{\mu\nu}$ matrices space is not reproducible.

At this point, it is not known why the parity violation that appears to be present in Fig. 4-4 is not reproducible. We posited that the average of the $(c_{Q,U,D})_{\mu\nu}$ was being done is over both the Gaussian fluctuations and the true parity violating signals, minimizing the effects of the parity violation. However, repeating our reproducibility studies taking all $(c_{Q,U,D})_{\mu\nu}$ instantiations that were significantly positive or negative to between (5-8)σ, still resulted in no evidence of chiral physics. Similarly, replacing the averaging process with simply taking the first $(c_{Q,U,D})_{\mu\nu}$ matrices instantiation that was significant to 4σ made no difference.

In summary: we have considered two models of physics inspired by the mSME, both with the ability to violate parity in the quark sector. In the first "effecitive momentum transformation"

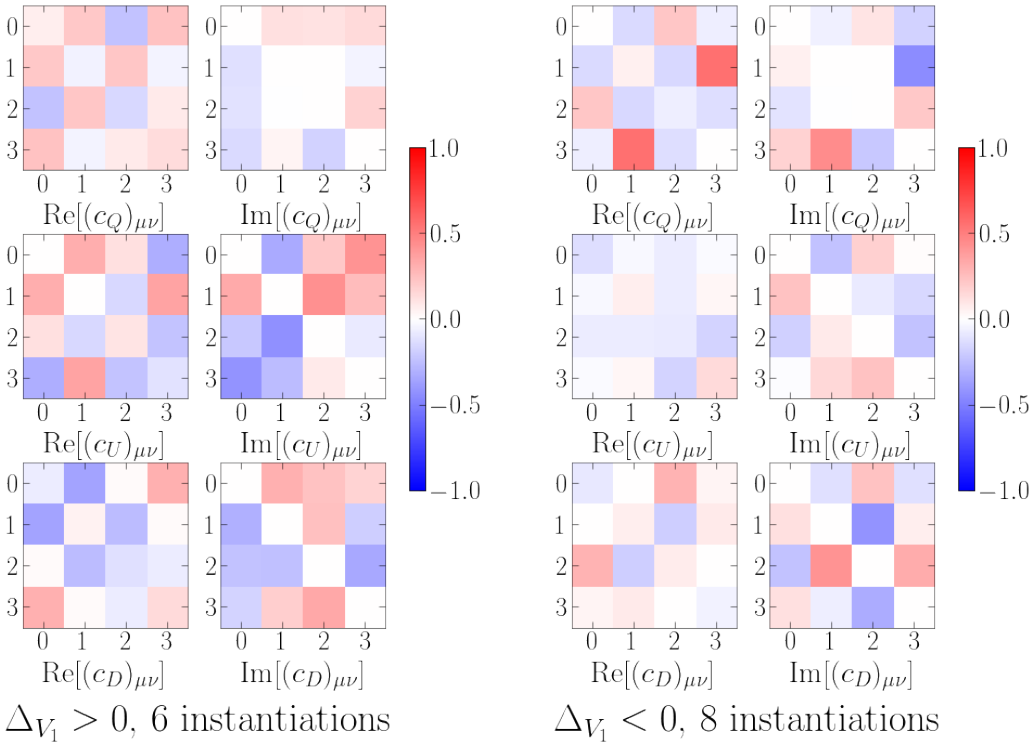

(a) Positive anomalies

(b) Negative anomalies

Figure 4-6: $(c_{Q,U,D})_{\mu\nu}$ matrices averaged over the instantiations gauged to be anomalous in V_1 (nonzero to between (4-8)σ). The number of instantiations of each case can be confirmed by looking at Fig. 4-4.

model, we found that our transformation coefficients $c_{\mu\nu}$ were able to produce parity-violating signatures for diagonal matrices, but not for certain off-diagonal ones. In our second single-diagram model, we found certain combinations of $(c_{Q,U,D})_{\mu\nu}$ that appeared anomalous at first pass, but did not continue to produce parity-violating physics for different kinematical setups.

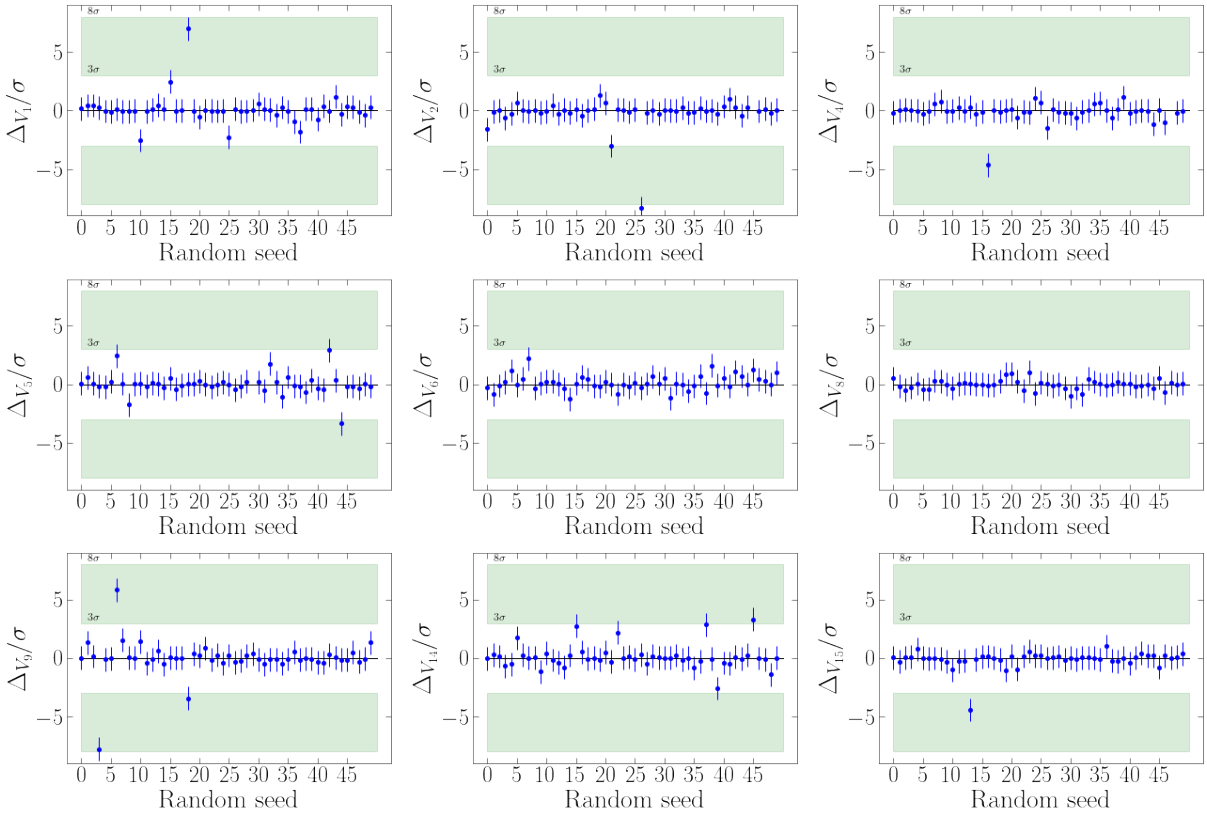

Figure 4-7: Δ_{V_i}/σ for the reproducibility studies. Each variable's subplot has been generated from 50 runs (each with a different random seed) on the same $(c_{Q,U,D})_{\mu\nu}$ setup, which has been chosen as the average of all matrix instantiations that are positively anomalous in that variable to between (4-8)σ.

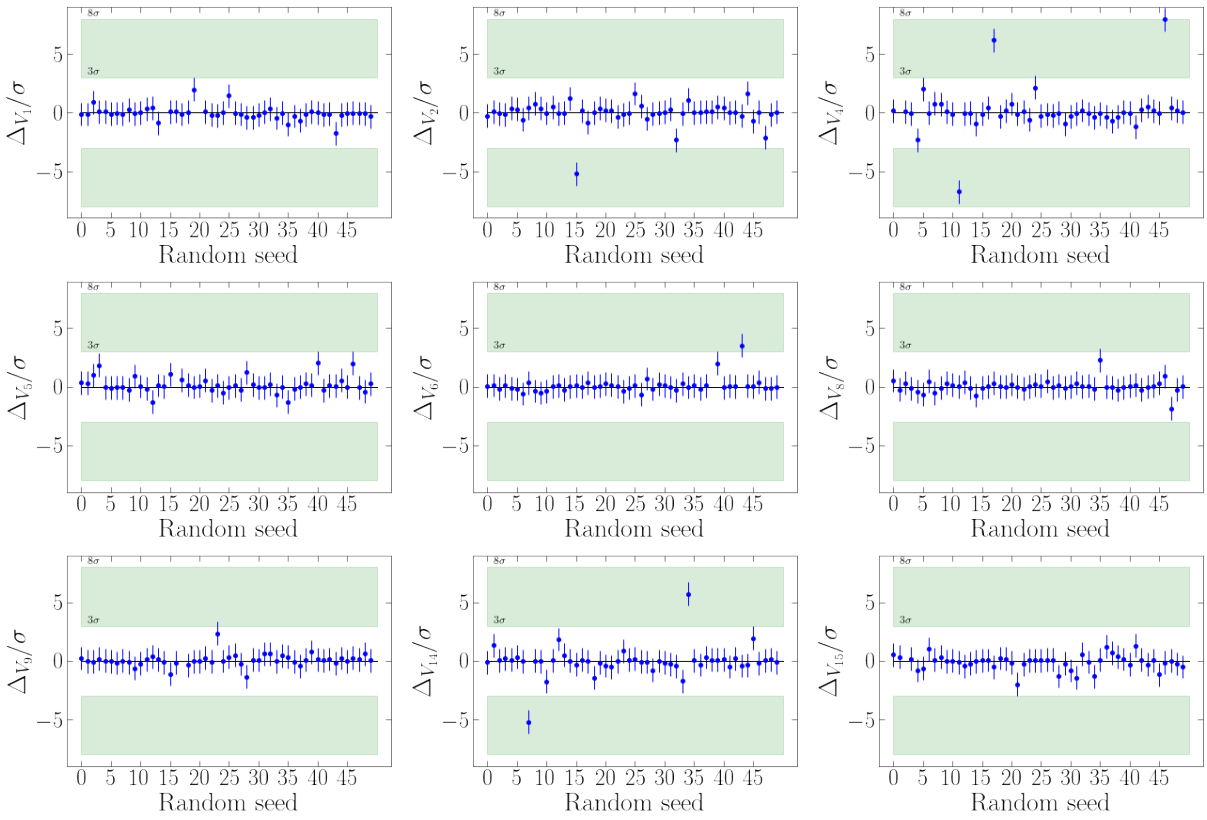

Figure 4-8: Same as Fig. 4-8, but generated from negative anomalies.

Chapter 5

Conclusions and Further Studies

In this report, we have evaluated the usefulness of the information provided by a set of *parity variables* designed to flag parity-violating processes for proton-proton collisions. We first tested the parity variables on the "Two spoons and a fork" model, a model designed to have parity violation controlled by a single scan parameter. We then introduced the Lorentz-violating minimal Standard Model Extension (mSME) and showed that such a model could violate parity for quark-gluon collisions. We finally explored two toy models of physics motivated by the mSME, finding only a lukewarm link between coefficients of the mSME background tensors and a signal in the parity variables. Clearly, there is still some work to be done before the parity variables could be used to search for new mSME physics at the LHC. At this point, it is not known whether this failure lies in the coding of the physics simulation, the discerning power of the parity variables, or in some other aspect.

Further studies should focus on targeting the source of this "parity leakage". The number of anomalies in Fig. 4-4 is greater than would be expected for a Gaussian distribution, implying that at least a few of the $(c_{Q,U,D})_{\mu\nu}$ instantiations would be truly parity-violating. Perhaps the problem could have been fixed with more computational time: 1,000 instantiations of the $(c_{Q,U,D})_{\mu\nu}$ matrices to explore a 45-dimensional space might have been too few to hone in on the most important couplings for parity violation. In addition, reproducibility studies run on 100 random seeds (rather than 50) may have provided more information. We would encourage future studies to devote more computational resources to exploring the $(c_{Q,U,D})_{\mu\nu}$ coupling space (potentially with a more methodical probe than the "bogoscan" method used in this report). We also recommend that future studies explore $2 \to 3$ diagrams other than the $ud \to udg$ one considered in this report.

If we take a moment to criticize the variables, rather than the simulation: perhaps the meta-variable Δ_{V_i} is not specific enough – if the *shape* of a histogram of parity variables were

asymmetric about the vertical axis, this would also be a nonzero signal that our meta-variable is insensitive to. Since the parity variables are proven in Ref. [19] to cover the complete $2 \to 3$ collision event space, it is more likely that the error lies on the side of the simulation, rather than that of the variables.

Assuming the parity leakage could be found, it would be useful to conduct tests on a more realistic version of the third model. But there are several barriers to making the computational model described in Chap. 4.2 more realistic within the scope of the mSME. We considered a single Feynman diagram for the process $ud \to udg$. However, collisions at the LHC are much more complex. A complete study would consider the sum of the hundreds of Feynman diagrams for the process $pp \to jjj$.

The largest challenge encountered in this project relates to this issue of simulating realistic mSME events. One might wonder why we used custom event generators in Chap. 4 instead of commonly used particle generators. Indeed, in the early stages of this project, a good deal of time was spent trying to implement the mSME Feynman rules into standard particle generators. However, the vast majority of these generators (such as FeynCalc [21] and LanHEP [22]) did not allow for the implementation of the custom Lorentz structures inherent in the mSME matrix elements. The only generator that did allow for user-defined vertices of this form was MadGraph [23]; however, it was later found that in the actual event generation calculations, MadGraph assumes Lorentz invariance and other fundamental symmetries in an attempt to save computational time (despite being given a manifestly Lorentz-violating matrix element). We therefore coded our own event generators, which are admittedly limited in scope.

Perhaps the most interesting finding is that the parity variables may be redundant. Indeed, the authors of Ref. [19] state that while all 19 of their variables are necessary for a complete cover of the $2 \to 3$ collision space, there may exist another complete cover with fewer variables. In our own quark-sector mSME studies (as evidenced in every figure in Chap. 4), we found that variables V_1 and V_2 provide the same information, as do the pairs V_8 and V_9, and V_{14} and V_{15}. As an explanation: the algebraic formulae for V_1 and V_2 are equivalent, barring a transformation from sums of Lorentz products in V_1 to products of those Lorentz products in V_2[1]. Similarly, V_8 and V_9 are complex conjugates of each other (as are V_{14} and V_{15}).

We encourage those working on experiments searching for parity violation at the LHC to also perform analyses based on these 19 parity variables. In addition to gauging more insights into the parity of certain proton-proton collisions, researchers will put the parity variables to

[1] V_1 contains terms $\epsilon^{ab}_{pq} + \epsilon^{bc}_{pq} + \epsilon^{ca}_{pq}$; V_2 contains terms $\epsilon^{ab}_{pq}\epsilon^{bc}_{pq}\epsilon^{ca}_{pq}$ where ϵ^{ab}_{pq} is a 4-dimensional determinant over daughter momenta a, b (and sometimes c) and mother momenta p, q. Refer to Ref. [19] for the long forms of all variables.

practical use and therefore hone in on what parts of the $2 \to 3$ phase space have redundancies in the parity variables. This could eventually lead to the determination of a more compact and complete cover of the $2 \to 3$ collision space. The new compact parity variables set could be calculated in tandem with every LHC search for new physics. The variables would be especially well-suited for model-agnostic BSM searches, as they function as flag for parity violation of any form with minimal computational overhead.

Appendix A

Deriving a manifestly parity-violating mSME Lagrangian

In this section, we will show that CPT-even quark sector minimal Standard Model Extension, as postulated in Ref. [16], can be split into the manifestly "vector+axial" form given in Eq. (3.2). The latter form is a more intuitive framework for conducting studies of parity violation, as the scale of parity violation in a given process corresponds directly to the relative size of that Lagrangian's vector and axial terms.

Let us restrict ourselves to two-flavor QCD, considering just the up and the down quarks. The relevant mSME Lagrangian is

$$\mathcal{L}_{\text{quark}}^{\text{CPT-even}} = \frac{1}{2} i\{(c_Q)_{\mu\nu AB}\overline{Q}_A\gamma^\mu \overleftrightarrow{D}^\nu Q_B + (c_U)_{\mu\nu AB}\overline{U}_A\gamma^\mu \overleftrightarrow{D}^\nu U_B + (c_D)_{\mu\nu AB}\overline{D}_A\gamma^\mu \overleftrightarrow{D}^\nu D_B\} \quad \text{(A.1)}$$

where $Q_A = \begin{pmatrix} u_A \\ d_A \end{pmatrix}_L$, $U_A = \left(u_A\right)_R$, and $D_A = \left(d_A\right)_R$.

For simplicity, we will assume the SME coefficients do not allow for flavor mixing (so we can neglect the A, B subscripts).

Expanding out the Lagrangian, we have

$$
\begin{aligned}
\mathcal{L}^{\text{CPT-even}}_{\text{quark}} =& \frac{1}{2} i\{(c_Q)_{\mu\nu}\overline{Q}\gamma^\mu \overleftrightarrow{D^\nu} Q + (c_U)_{\mu\nu}\overline{U}\gamma^\mu \overleftrightarrow{D^\nu} U + (c_D)_{\mu\nu}\overline{D}\gamma^\mu \overleftrightarrow{D^\nu} D\} \\
=& \frac{1}{2} i\{(c_Q)_{\mu\nu}\overline{u_L}\gamma^\mu \overleftrightarrow{D^\nu} u_L + (c_Q)_{\mu\nu}\overline{d_L}\gamma^\mu \overleftrightarrow{D^\nu} d_L \\
& + (c_U)_{\mu\nu}\overline{u_R}\gamma^\mu \overleftrightarrow{D^\nu} u_R + (c_D)_{\mu\nu}\overline{d_R}\gamma^\mu \overleftrightarrow{D^\nu} d_R\} \\
=& \frac{1}{2} i\{(c_Q)_{\mu\nu}\overline{(P_L u)}\gamma^\mu \overleftrightarrow{D^\nu} (P_L u) + (c_Q)_{\mu\nu}\overline{(P_L d)}\gamma^\mu \overleftrightarrow{D^\nu} (P_L d) \\
& + (c_U)_{\mu\nu}\overline{(P_R u)}\gamma^\mu \overleftrightarrow{D^\nu} (P_R u) + (c_D)_{\mu\nu}\overline{(P_R d)}\gamma^\mu \overleftrightarrow{D^\nu} (P_R d)\} \\
=& \frac{1}{2} i\{(c_Q)_{\mu\nu}\overline{u}\gamma^\mu \overleftrightarrow{D^\nu} (1-\gamma^5) u + (c_U)_{\mu\nu}\overline{u}\gamma^\mu \overleftrightarrow{D^\nu} (1+\gamma^5) u \\
& + (c_Q)_{\mu\nu}\overline{d}\gamma^\mu \overleftrightarrow{D^\nu} (1-\gamma^5) d + (c_D)_{\mu\nu}\overline{d}\gamma^\mu \overleftrightarrow{D^\nu} (1+\gamma^5) d \\
=& \frac{1}{2} i\{[(c_Q)_{\mu\nu} + (c_U)_{\mu\nu}]\overline{u}\gamma^\mu \overleftrightarrow{D^\nu} u + [-(c_Q)_{\mu\nu} + (c_U)_{\mu\nu}]\overline{u}\gamma^\mu \overleftrightarrow{D^\nu} \gamma^5 u \\
& + [(c_Q)_{\mu\nu} + (c_D)_{\mu\nu}]\overline{d}\gamma^\mu \overleftrightarrow{D^\nu} d + [-(c_Q)_{\mu\nu} + (c_D)_{\mu\nu}]\overline{d}\gamma^\mu \overleftrightarrow{D^\nu} \gamma^5 d
\end{aligned}
\tag{A.2}
$$

We now define some vector and axial couplings:

$$
\begin{aligned}
(c_{V,u})_{\mu\nu} &= +(c_Q)_{\mu\nu} + (c_U)_{\mu\nu} \\
(c_{A,u})_{\mu\nu} &= -(c_Q)_{\mu\nu} + (c_U)_{\mu\nu} \\
(c_{V,d})_{\mu\nu} &= +(c_Q)_{\mu\nu} + (c_D)_{\mu\nu} \\
(c_{A,d})_{\mu\nu} &= -(c_Q)_{\mu\nu} + (c_D)_{\mu\nu}
\end{aligned}
\tag{A.3}
$$

Then our Lagrangian can be re-written as

$$
\begin{aligned}
&\mathcal{L}^{\text{CPT-even}}_{\text{quark}} = \\
&\frac{1}{2} i\{(c_{V,u})_{\mu\nu}\overline{u}\gamma^\mu \overleftrightarrow{D^\nu} u + (c_{A,u})_{\mu\nu}\overline{u}\gamma^\mu \overleftrightarrow{D^\nu} \gamma^5 u + (c_{V,d})_{\mu\nu}\overline{d}\gamma^\mu \overleftrightarrow{D^\nu} d + (c_{A,d})_{\mu\nu}\overline{d}\gamma^\mu \overleftrightarrow{D^\nu} \gamma^5 d\}
\end{aligned}
\tag{A.4}
$$

Let's compare this with the Standard Model Lagrangian, which is given by

The Standard Model Lagrangian for the quark sector is given by the following expression:

$$
\begin{aligned}
\mathcal{L}^{\text{SM}}_{\text{quark}} =& \frac{1}{2} i\overline{Q}_A \gamma^\mu \overleftrightarrow{D_\mu} Q_A + \frac{1}{2} i\overline{U}_A \gamma^\mu \overleftrightarrow{D_\mu} U_A + \frac{1}{2} i\overline{D}_A \gamma^\mu \overleftrightarrow{D_\mu} D_A \\
=& \frac{1}{2} i\{(c_{V,u})\overline{u}\gamma^\mu \overleftrightarrow{D_\mu} u + (c_{A,u})\overline{u}\gamma^\mu \overleftrightarrow{D_\mu} \gamma^5 u + (c_{V,d})\overline{d}\gamma^\mu \overleftrightarrow{D_\mu} d + (c_{A,d})\overline{d}\gamma^\mu \overleftrightarrow{D_\mu} \gamma^5 d\}
\end{aligned}
\tag{A.5}
$$

with $(c_{V,u}) = (c_{V,d}) = 2, (c_{A,u}) = (c_{A,d}) = 0$.

Bibliography

[1] C. S. Wu et al. "Experimental Test of Parity Conservation in β Decay". In: *Phys. Rev.* 105 (1957), pp. 1413–1414. DOI: 10.1103/PhysRev.105.1413.

[2] J. H. Christenson et al. "Evidence for the 2π Decay of the K_2^0 Meson". In: *Phys. Rev. Lett.* 13 (1964), pp. 138–140. DOI: 10.1103/PhysRevLett.13.138.

[3] Roel Aaij et al. "Test of lepton universality in beauty-quark decays". In: (Mar. 2021). arXiv: 2103.11769 [hep-ex].

[4] Daljeet Kaur. "CPT violation sensitivity of NoVA, T2K and INO experiments using ν and $\bar{\nu}$ oscillation parameters". In: *PoS* ICHEP2020 (2021), p. 204. DOI: 10.22323/1.390.0204.

[5] F. N. Diaz Desposorio, Juan Carrasco-Martinez, and Alberto Gago. "Neutrino oscillation and CPT violation due to quantum decoherence at DUNE". In: *PoS* EPS-HEP2019 (2020), p. 384. DOI: 10.22323/1.364.0384.

[6] B. Quinn. "CPT- and Lorentz-Violation Tests with Muon g-2". In: *8th Meeting on CPT and Lorentz Symmetry*. June 2019. DOI: 10.1142/9789811213984_0044. arXiv: 1907.00162 [hep-ex].

[7] Aleksander Gajos. "Sensitivity of Discrete Symmetry Tests in the Positronium System with the J-PET Detector". In: *Symmetry* 12.8 (2020), p. 1268. DOI: 10.3390/sym12081268. arXiv: 2006.01012 [physics.ins-det].

[8] C. Bartram and R. Henning. "Caliope: a search for CPT-violation in o-ps". In: *J. Phys. Conf. Ser.* 1342.1 (2020). Ed. by Ken Clark et al., p. 012106. DOI: 10.1088/1742-6596/1342/1/012106.

[9] Victor Mukhamedovich Abazov et al. "Direct measurement of the mass difference between top and antitop quarks". In: *Phys. Rev. D* 84 (2011), p. 052005. DOI: 10.1103/PhysRevD.84.052005. arXiv: 1106.2063 [hep-ex].

[10] Antonio Di Domenico. "Testing CPT Symmetry with Neutral K Mesons: A Review". In: *Symmetry* 12.12 (2020), p. 2063. DOI: 10.3390/sym12122063.

[11] E. De Lucia. "CPT Symmetry Test at KLOE-2". In: *J. Phys. Conf. Ser.* 1526.1 (2020). Ed. by Patrizia Cenci and Mauro Piccini, p. 012006. DOI: 10.1088/1742-6596/1526/1/012006.

[12] Andrew S. Friedman et al. "Improved constraints on anisotropic birefringent Lorentz invariance and CPT violation from broadband optical polarimetry of high redshift galaxies". In: *Phys. Rev. D* 102.4 (2020), p. 043008. DOI: 10.1103/PhysRevD.102.043008.

[13] G. Lüders. "Det. Kong. Danske Videnskabernes Selskab". In: *Mat.-fys. Medd.* 28, No. 5 (1954).

[14] W. Pauli. In: *Niels Bohr and the Development of Physics* ((McGraw-Hill, New York). 1955. pp30-51), pp. 30–51.

[15] Robert Bluhm. ""Breaking Lorentz symmetry"". In: *Physics World, IOP Publishing* (29 Aug. 2018). URL: physicsworld.com%5C/breaking-lorentz-symmetry%5C/.

[16] Don Colladay and V.Alan Kostelecky. "Lorentz violating extension of the standard model". In: *Phys. Rev. D* 58 (1998), p. 116002. DOI: 10.1103/PhysRevD.58.116002.

[17] Don Colladay and V. Alan Kostelecky. "CPT violation and the standard model". In: *Phys. Rev. D* 55 (1997), pp. 6760–6774. DOI: 10.1103/PhysRevD.55.6760. arXiv: hep-ph/9703464.

[18] V. Alan Kostelecky and Neil Russell. "Data Tables for Lorentz and CPT Violation". In: (Jan. 2008). arXiv: 0801.0287 [hep-ph].

[19] Christopher G. Lester, Ward Haddadin, and Ben Gripaios. "Lorentz and permutation invariants of particles III: constraining non-standard sources of parity violation". In: (Aug. 2020). arXiv: 2008.05206 [hep-ph].

[20] V. Alan Kostelecký et al. "Lorentz and CPT Violation in Partons". In: *JHEP* 04 (2020), p. 143. DOI: 10.1007/JHEP04(2020)143. arXiv: 1911.04002 [hep-ph].

[21] Vladyslav Shtabovenko. "FeynCalc 9". In: *J. Phys. Conf. Ser.* 762.1 (2016). Ed. by Luis Salinas and Claudio Torres, p. 012064. DOI: 10.1088/1742-6596/762/1/012064. arXiv: 1604.06709 [hep-ph].

[22] A. Semenov. "LanHEP — A package for automatic generation of Feynman rules from the Lagrangian. Version 3.2". In: *Comput. Phys. Commun.* 201 (2016), pp. 167–170. DOI: 10.1016/j.cpc.2016.01.003. arXiv: 1412.5016 [physics.comp-ph].

[23] J. Alwall et al. "The automated computation of tree-level and next-to-leading order differential cross sections, and their matching to parton shower simulations". In: *JHEP* 07 (2014), p. 079. DOI: 10.1007/JHEP07(2014)079. eprint: 1405.0301.